APPENDIX

N number of atoms in the unit cell
$E_{\mathbf{h}}$ normalized structure factor
$R_{\mathbf{h}}$ magnitude of the normalized structure factor
$\varepsilon_{\mathbf{h}}$ $R_{\mathbf{h}}^2 - 1$
$\mathbf{C}_p$ $\{\mathbf{R}_p, \mathbf{T}_p\}$, pth symmetry operator
$\mathbf{R}_p$ pth rotation matrix of the point group
$\mathbf{T}_p$ translation vector associated with the pth rotation matrix of the point group
I identity 3×3 matrix
$I_0(x), I_1(x)$ modified Bessel functions of order zero and one respectively
$L_4(x) = x^4 - 4x^2 + 2$ Laguerre polynomial of order 4
s.s. structure seminvariant.

References

ARORA, S. K., GERMAIN, G. & DECLERCQ, J. P. (1976). *Acta Cryst.* B**32**, 415–419.

BRAEKMAN, J. C., DALOZE, D., DUPONT, A., TURSCH, B., DECLERCQ, J. P., GERMAIN, G. & VAN MEERSSCHE, M. (1981). *Tetrahedron*, **37**, 179–186.

BURLA, M. C., NUNZI, A., GIACOVAZZO, C. & POLIDORI, G. (1981). *Acta Cryst.* A**37**, 677–684.

BUSETTA, B., GIACOVAZZO, C., BURLA, M. C., NUNZI, A., POLIDORI, G. & VITERBO, D. (1980). *Acta Cryst.* A**36**, 68–74.

COLENS, A., DECLERCQ, J. P., GERMAIN, G., PUTZEYS, J. P. & VAN MEERSSCHE, M. (1974). *Cryst. Struct. Commun.* **3**, 119–122.

DECLERCQ, J. P., GERMAIN, G. & VAN MEERSSCHE, M. (1972). *Cryst. Struct. Commun.* **1**, 13–15.

GIACOVAZZO, C. (1976). *Acta Cryst.* A**32**, 958–967.

GIACOVAZZO, C. (1977). *Acta Cryst.* A**33**, 933–944.

GIACOVAZZO, C. (1979). *Acta Cryst.* A**35**, 296–305.

GIACOVAZZO, C. (1980*a*). *Acta Cryst.* A**36**, 362–372.

GIACOVAZZO, C. (1980*b*). *Direct Methods in Crystallography*. London: Academic Press.

GIACOVAZZO, C. (1980*c*). *Acta Cryst.* A**36**, 704–711.

GIACOVAZZO, C., SPAGNA, R., VICKOVIĆ, I. & VITERBO, D. (1979). *Acta Cryst.* A**35**, 401–412.

GIACOVAZZO, C. & VICKOVIĆ, I. (1980). *Acta Cryst.* A**36**, 1017–1025.

KARLE, I. L., KARLE, J. & ESTLIN, J. A. (1967). *Acta Cryst.* **23**, 494–500.

Acta Cryst. (1982). A**38**, 670–679

Low-Resolution Neutron Diffractometry with a Position-Sensitive Multidetector

BY MICHEL ROTH AND ANITA LEWIT-BENTLEY*

Institut Laue–Langevin, 156X, Centre de Tri, 38042 *Grenoble CEDEX, France*

(*Received* 19 *November* 1981; *accepted* 8 *April* 1982)

Abstract

A data reduction system for neutron crystallography using a two-dimensional planar multidetector is described. The method is based on an *a priori* calculation of the intensity distribution for each reflection for any crystal orientation. The orientation matrix of the crystal has to be known. From the calculated intensity distribution a mask is derived for each reflection. The detection elements of the detector which are inside the mask are summed to determine the intensity of that reflection and the cells outside are used to determine the background. The size of the mask is adapted to the relative height of the measured intensity of the reflector compared to the background. The theoretical intensity distribution for each reflection is calculated in reciprocal space from the primary-beam divergence and wavelength spread and the crystal mosaic spread, on the basis of the kinematic theory of diffraction. The derivation of the necessary equations, *i.e.* the determination of the resolution function of the instrument, is presented. Some typical results of data collection are also presented. The advantages of this data collection method are the safe determination of weak reflections, the easy discrimination of reflections which nearly overlap, the determination of crystal mosaic spread, and the discrimination of inelastic scattering in the proximity of intense reflections.

1. Introduction

Low-resolution neutron crystallography using H_2O/D_2O contrast variation is establishing itself as a useful

* Present address: EMBL, Grenoble Outstation, 156X, Centre de Tri, 38042 Grenoble CEDEX, France.

0567-7394/82/050670-10$01.00

method of determining the structures of two-component biological molecules, such as viruses and the nucleosome core particle (Bentley, Finch & Lewit-Bentley, 1981). These molecules usually form small crystals (<1 mm in the largest dimension) with large unit cells (100–400 Å) and would thus require large neutron fluxes. With long wavelengths (~10 Å), however, the increased reflectivity of the crystals (of about two orders of magnitude) will compensate, to a large extent, for low fluxes. The use of a position-sensitive two-dimensional multidetector further increases the efficiency of data collection.

Long-wavelength neutrons are monochromated by velocity selectors which give a fairly large wavelength spread ($\Delta\lambda/\lambda$) of 4–10% (full width at half height, FWHH). A considerable beam divergence (up to 2°) can be maintained to maximize the neutron flux, provided it does not limit the resolving power of the instrument for a given crystal. Together with the crystal mosaicity, however, these effects cause a large spread of reflections which has to be taken into account for accurate intensity measurements.

Position-sensitive multidetectors are being used increasingly for X-ray and neutron crystallography (Xuong, Freer, Hamlin, Nielsen & Vernon, 1978; Spencer & Kossiakoff, 1980; Sjölin & Wlodawer, 1981). Successful data reduction requires the prediction of the position of reflections on each successive data frame (spectrum). With proteins, where the majority of reflections are weak, more accurate data can be obtained if the reflection shape is predicted as well as its position. In this paper we present a method of calculating a reflection shape from the measured properties of the incident beam, the measurable mosaic spread of the crystals and the known behaviour of the diffracted beam. We call this method the 'resolution-function' method, to distinguish it from those that use an empirical, learned shape. The term resolution function was defined for double-crystal diffractometers with single counters by Cooper & Nathans (1967, 1968) and Lebech & Nielsen (1975) as a function measuring 'for a fixed setting of the diffractometer, a spread of the incoming and scattered wave vectors around their average values'. In our case it is the distribution of the diffracted intensity on a two-dimensional detector as a function of the crystal orientation that is calculated. The experimental conditions used in the present work, *i.e.* a velocity selector for monochromation of neutrons, no collimation slits, a rather large beam divergence and wavelength spread, differ from those used in standard neutron diffractometry and the calculation of the intensity distribution is therefore different too. It is worth noting, though, that the calculations presented here are not restricted to Gaussian approximations as is the case for the earlier resolution-function calculations. Gaussian approximations are introduced nevertheless in order to speed up calculation time on a computer. The strength of any resolution-function method is that it predicts *a priori* the shape of a reflection and thus weak reflections can be treated as reliably as strong ones. We may evaluate overlap between reflections where that occurs and, in addition, study any departure of experimental data from the theoretical reflection shape.

2. Instrument geometry

The instrument used for data collection is the small-angle scattering camera D17 at the Institute Laue–Langevin. It is installed at the exit of a curved neutron guide (H17) with a wavelength spectrum of 8–20 Å. The maximum flux at the sample is $\sim 10^6$ n s^{-1} cm^{-2} at $\lambda = 11$ Å, the beam divergence about 0·5–1° (FWHH). The beam is monochromated by a helical

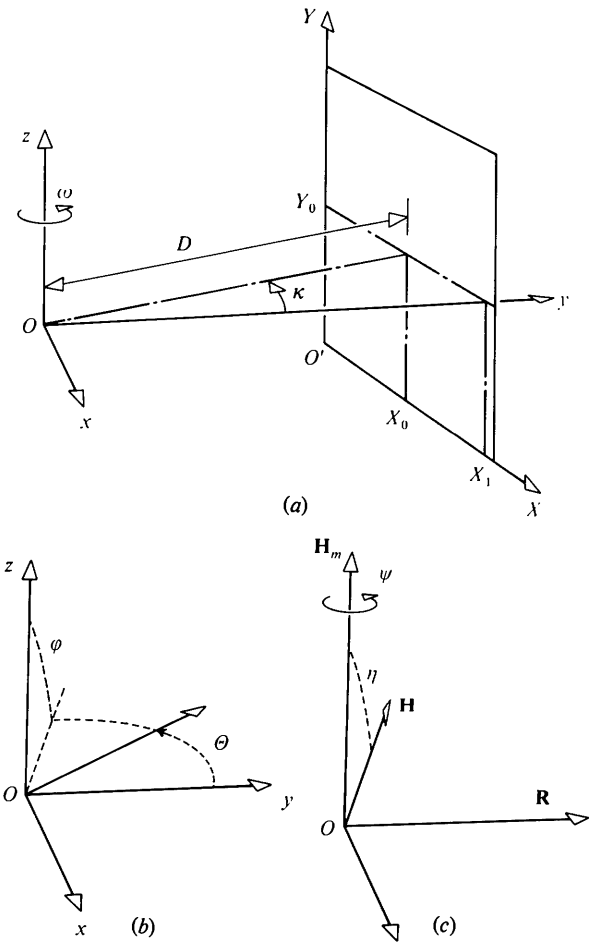

Fig. 1. Definition of coordinates. (*a*) Instrument coordinates: *Oy* is the direction of the incident beam. The detector (coordinates *O'XY*) is rotated by an angle κ from **y** around the vertical **z**. The distance *D* between the sample (at *O*) and the detector is determined by measuring the variation of X_1 as a function of κ. (*b*) Diffraction coordinates Θ,φ in the system *Oxyz*. (*c*) Mosaicity rotations η and ψ of **H** with respect to $\mathbf{H}_m$.

slot velocity selector which gives a wavelength spread ($\Delta\lambda/\lambda$) of 10% (FWHH). A 4·5% (FWHH) selector is also available with, however, a 50% loss of flux.

D17 is equipped with a LETI BF_3-filled multiwire planar multidetector, 64 × 64 cm with 16 384 detection elements of 0·5 × 0·5 cm each. At the moment the 1 × 1 cm grid option is used for collecting crystal data. The detector can be positioned at 0·8, 1·5, or 2·8 m from the sample and rotated horizontally about the sample position from 0 to 90°.

For single-crystal experiments a full-circle Eulerian cradle has been installed to allow crystal orientation. The normal beam geometry is used for data collection, with an ω step scan and Φ,χ and detector rotation angle (κ) fixed. The axial system was defined using the conventions of Busing & Levy (1967), with **y** parallel to the incident beam, **z** vertical (coincident with the crystal rotation axis) and **x** completing a right-handed orthogonal axial system. The axial systems are summarized in Fig. 1. The crystal is assumed to be placed at the origin of the reference system of axes.

The intensity distribution in the main beam is determined experimentally: with no crystal in the sample position the counts on the detector (*i.e.* at a distance $y = D$ from the sample) are evaluated to give the distribution as a function of x and z in the axial system defined above. The distribution of intensity as a function of wavelength is determined from a time-of-flight measurement. When the beam is monochromated by a velocity selector the wavelength dependence of the intensity can be represented by a triangular distribution (Fig. 2) (Ibel, 1976). At the exit from the velocity selector, the value of the wavelength is somewhat dependent on the direction of the beam, as in the case of crystal monochromators. This effect is attenuated on D17 by a 3 m neutron guide placed between the selector and the sample, and can therefore be neglected. The dimensions of the crystals used are always of the order of a millimetre or smaller and are thus small compared with the sample-to-detector distance D (≥0·8 m) and to the detector resolution (0·5 or 1 cm). It is therefore reasonable to approximate the sample by a point crystal. For a given wavelength λ, on a given point of the detector, the intensity of the incident beam corresponds to a given vector $\mathbf{k}_0$ with coordinates

$$(k_0)_x = 2\pi x/\lambda D, \quad (k_0)y = 2\pi/\lambda, \quad (k_0)_z = 2\pi z/\lambda D \quad (1)$$

in reciprocal space.

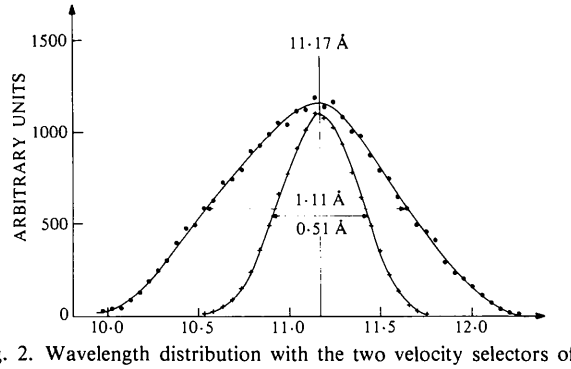

Fig. 2. Wavelength distribution with the two velocity selectors of the spectrometer D17. The inner and the outer curves correspond to 4·5 and 10% FWHH respectively.

3. Diffracted intensity

3.1. *General considerations*

To calculate the intensity diffracted by a crystal we use the kinematic theory of diffraction, *i.e.* the approximation of an ideally imperfect crystal. This approximation seems to be quite reasonable with regard to the determination of the size of the reflections.

We also neglect the influence of the mosaic blocks assuming that their size, d, is significantly larger than 0·1 μm ($\lambda/d \ll 10^{-2}$).

Under these conditions the scattering cross section of a crystal can be expressed as a sum of Dirac functions $\delta(\mathbf{Q} - \mathbf{H})$. Here $\mathbf{Q}$ is the scattering vector:

$$\mathbf{Q} = \mathbf{k} - \mathbf{k}_0, \quad (2)$$

where $\mathbf{k}_0$ and $\mathbf{k}$ are the incoming and outgoing wave vectors of neutrons respectively and $k = k_0 = 2\pi/\lambda$ (elastic scattering).

3.2. *Calculation of diffracted intensity for zero mosaic spread*

We want to determine the number of neutrons δn scattered within a solid angle $\delta\Omega$ in the direction Θ,φ for a given vector $\mathbf{H}$ (corresponding to a reflection hkl). This number can be expressed as a function of the incident beam $i(z,x,\lambda)$ (Lomer & Low, 1965):

$$\delta n(\Theta,\varphi) = \frac{(2\pi)^3 N}{V} |F(\mathbf{H})|^2 \, \delta\Omega T \times \int \delta(\mathbf{Q} - \mathbf{H}) \, i(z,x,\lambda) \, dz \, dx \, d\lambda, \quad (3)$$

where N = number of unit cells in the crystal, T is the transmission in the direction Θ,φ, Θ,φ are the spherical coordinates related to the axial system **z**,**x**,**y** (Fig. 1*b*).

The diffraction vector $\mathbf{Q}$ is a function of z, x, λ, Θ and φ. In order to evaluate the integral in (3) it is useful to change the variables z,x,λ into Q_z,Q_x,Q_y by calculating the Jacobian:

$$J = \frac{\partial(z,x,\lambda)}{\partial(Q_z,Q_x,Q_y)}. \quad (4)$$

From (1), (2) and using Bragg's law expressed in the form

$$\mathbf{Q}.\mathbf{k} = Q^2/2, \quad (5)$$

we obtain the following relationships:

$$z = D[\sin\Theta\cos\varphi - (\lambda/2\pi)\,Q_z]$$
$$x = D[\sin\Theta\sin\varphi - (\lambda/2\pi)\,Q_x] \qquad (6)$$
$$\lambda = (4\pi/Q^2)\,\mathbf{Q}.\mathbf{k}/k_0,$$

and thus

$$J = (\lambda/2\pi)^2\,D^2\left|\frac{\partial\lambda}{\partial Q_y}\right|, \qquad (7)$$

which can be rewritten as

$$J = (2/Q^2)(\lambda/2\pi)^2\,D^2|\cos\Theta - Q_y\,\lambda/2\pi|. \qquad (8)$$

Introducing the Jacobian (8) into (3) and evaluating the integral we obtain:

$$\delta n(\Theta,\varphi) = N_0|F|^2\,\delta\Omega T 2[\lambda^*\,D/(2\pi H)]^2 \times |\cos\Theta - H_y\,\lambda/2\pi|\;i(z^*,x^*,\lambda^*), \qquad (9)$$

where

$$\lambda^* = (4\pi/H^2)(H_z\sin\Theta\cos\varphi + H_x\sin\Theta\sin\varphi + H_z\cos\Theta)$$
$$z^* = D[\sin\Theta\cos\varphi - (\lambda^*/2\pi)\,H_z] \qquad (10)$$
$$x^* = D[\sin\Theta\sin\varphi - (\lambda^*/2\pi)\,H_x]$$

and $N_0 = (2\pi)^3\,N/V$.

3.3. *Effects of mosaic spread*

In our calculation we have assumed a directionally isotropic distribution of mosaic blocks. The different orientations of a vector **H** for a reflection *hkl* are then described by a distribution function f_M of two parameters: one, η, is the angle between one of the directions of **H** and the mean direction $\mathbf{H}_m$ of the ensemble of vectors **H**. The other, ψ, is the rotation angle of **H** about $\mathbf{H}_m$ (Fig. 1*c*). The vector **H** is then derived from $\mathbf{H}_m$ using

$$\mathbf{H} = \mathbf{H}_m + \eta\mathbf{R}\times\mathbf{H}_m. \qquad (11)$$

Here **R** is a unit vector perpendicular to $\mathbf{H}_m$ whose direction is given by ψ. We are assuming here that the distribution function f_M depends only on η and is symmetrical about $\mathbf{H}_m$. Thus the final expression of $\delta n(\Theta,\varphi)$ is:

$$\delta n(\Theta,\varphi) = N_0|F|^2\,\delta\Omega T 2(D^2/H^2) \times \int f_M(\eta)(\lambda^*/2\pi)^2|\cos\Theta - H_y\,\lambda^*/2\pi| \times i(z^*,x^*,\lambda^*)\,\eta\,\mathrm{d}\eta\,\mathrm{d}\psi. \qquad (12)$$

4. Use of the intensity calculation

With (12) we may calculate the diffracted intensity in any direction (Θ,φ) for a given reflection *hkl* and a given crystal orientation. The magnitude of this intensity will obviously be zero everywhere except in close proximity to the direction corresponding to Bragg's law. In order to use (12) efficiently it is therefore necessary to estimate *a priori* the direction in which a given reflection fulfils Bragg's law for a given crystal orientation and then to calculate all values of $\delta n(\Theta,\varphi)$ in the proximity of that direction. It is thus useful to estimate the extent of the volume within which the calculation will be performed, especially the angular range of rotation of the crystal during which the reflection remains in a diffracting position. These estimates can be obtained from the geometry of diffraction.

The diffraction geometry in reciprocal space for a vector **H** is shown in Fig. 3. The figure is drawn in the plane of mean diffraction, containing the mean incident wave vector $(\mathbf{k}_0)_m$ and the vector **H**. The direct beam is represented by the hatched volume centred around $(\mathbf{k}_0)_m$ and comprising all vectors $\mathbf{k}_0$ that constitute the incident beam. The diffracted part of the incident beam is determined by the intersection of this volume with a

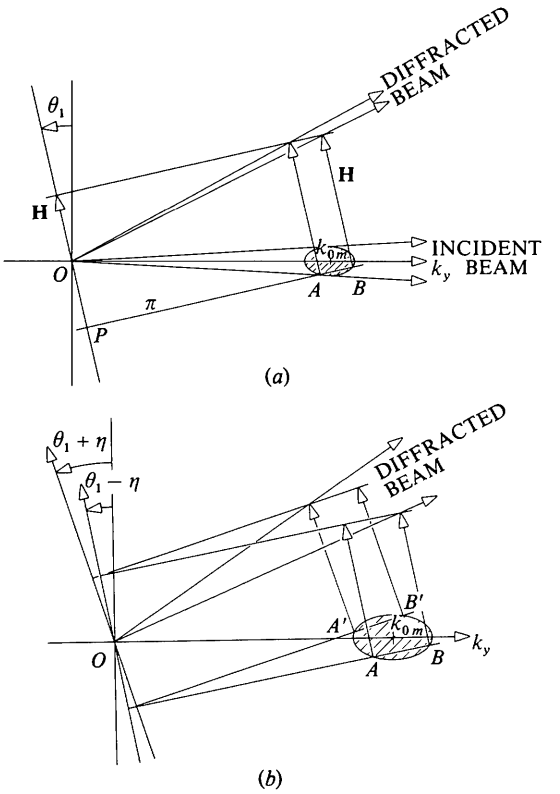

Fig. 3. Geometrical construction in reciprocal space of the diffracted beam in the mean diffraction plane (see text). (*a*) For a single vector **H**, *i.e.* for zero mosaicity. The only part of the incident beam effectively active in diffraction is the section *AB*. (*b*) With two vectors **H** to show the effect of the mosaic spread. The whole volume of incident beam included between the sections *AB* and *A' B'* contributes to diffraction.

plane π which is perpendicular to **H** and which passes through point P at $-\mathbf{H}/2$ from the origin. The diffracted beam is given by a vectorial translation of this intersection equal to **H**.

The width of the diffracted beam, measured in the plane of mean diffraction, is always smaller or at most equal to the angular width of the incident beam. This width is of course increased by the mosaicity of the crystal (Fig. 3*b*) but in a limited way for real crystals where the mosaic spread is smaller than 0·5° FWHH.

The transverse angular width of the diffracted beam, *i.e.* in a direction normal to the plane of mean diffraction, is about the same as the angular width of the incident beam.

4.1. *Gaussian approximation*

The Gaussian approximation is introduced by using the following expressions:

(1) the function

$$i(x,z,\lambda) = \exp[-(x^2 + z^2)/\sigma_\nu^2 D^2)] \exp[-(\lambda - \lambda_0)^2/\sigma_\lambda^2] \tag{13}$$

for the distribution of intensity in the main beam; this approximation holds well for the distribution in **x** and **z** but is less accurate for the distribution in λ;

(2) the function

$$f_M(\eta) = \exp(-\eta^2/\sigma_\eta^2) \tag{14}$$

for the distribution of mosaicity for all vectors **H** around the mean vector $\mathbf{H}_m$ for the given *hkl*.

The mean diffraction plane is defined by the **y** axis and the direction $\mathbf{H}_m$. Let φ_m be the angle of the **z** axis with this plane and θ_1 the angle between $\mathbf{H}_m$ and the *xz* plane (*i.e.* the plane normal to the beam). The relative value of intensity diffracted in a direction (Θ,φ) is given to a first approximation (if non-exponential factors are not considered) by

$$\delta n(\Theta,\varphi) = \exp[-(\sin\theta_1 - \sin\theta_0)^2/\sigma_1^2 - (\Theta - \Theta_m)^2/\sigma_\Theta^2 - (\varphi - \varphi_m)^2/\sigma_\varphi^2], \tag{15}$$

where θ_0 is the mean Bragg angle, and

$$\sigma_1^2 = (\sigma_\lambda^{*2} + \sigma_\nu^2 \cos^2\theta_1 + \sigma_\eta^2 \cos\theta_1)^2 \times (\sigma_\lambda^{*2} + \sigma_\nu^2 \cos^2\theta_1 + \sigma_\eta^2)^{-1} \tag{16}$$

$$\sigma_\lambda^* = (\sigma_\lambda/\lambda_0)\sin\theta_o \tag{17}$$

$$\Theta_m = 2\theta_1 + (\sin\theta_0 - \sin\theta_1)(2\sigma_\eta^2 + \sigma_\nu^2 \cos\theta_1) \times (\sigma_\lambda^{*2} + \sigma_\nu^2 \cos^2\theta_1 + \sigma_\eta^2 \cos\theta_1)^{-1} \tag{18}$$

$$\sigma_\Theta^2 = (\sigma_\nu^2 \sigma_\eta^2 \cos^2\theta_1 + 4\sigma_\lambda^{*2} \sigma_\eta^2 + \sigma_\lambda^{*2} \sigma_\nu^2) \times [(\sigma_\eta^2 + \sigma_\nu^2)\cos^2\theta_1 + \sigma_\lambda^{*2}]^{-1} \tag{19}$$

$$\sigma_\varphi^2 = \sigma_\eta^2 \cos^{-2}\theta_0 + 2\sigma_\nu^2 \sin^{-2} 2\theta_0. \tag{20}$$

The coordinates of maximum intensity for a given position of the crystal are Θ_m and φ_m. Because of the non-ideality of the incident beam and of the crystal mosaicity, the variation of Θ_m as a function of θ_1 departs noticeably from the ideal case of the $\Theta_m = 2\theta_1$ type. Fig. 4 shows the calculated variations of angular width (FWHH) of a reflection in the diffraction plane and in the transverse direction (proportional to σ_Θ and σ_φ respectively) as a function of the mean diffraction angle $2\theta_0$.†

Since diffraction takes place only for values of θ_1 close to θ_0, $\cos\theta_1$ can be replaced by $\cos\theta_0$ in the above relations. With a velocity selector the wavelength spread σ_λ/λ_0 is constant. It follows then that the angular widths σ_Θ and σ_φ of the reflections are independent of wavelength and depend only on the mean diffraction angle $2\theta_0$.

4.2. *Limits of the ω range*

The crystal data are measured using the normal beam geometry, with the crystal being rotated in steps about an axis perpendicular to the beam. The rotation axis is coincident with the **z** direction and the rotation of the crystal measured as ω. We assume that the orientation matrix of the crystal, the *UB* matrix, has been determined and thus the components H_x^*, H_y^*, H_z^* of any vector **H** of the crystal reciprocal lattice are known for $\omega = 0$. The components H_x, H_y, H_z for any value of ω can be calculated using a rotation matrix. In order to determine the ω range during which a reflection remains in the diffracting position we first consider the case of zero mosaicity.

Zero mosaic spread. As seen in Fig. 5, the two positions of vector **H** that are at the limits of the domain of diffraction are defined by the positions where the plane is tangent to the surface (S) that encloses the total volume in reciprocal space in which the intensity of the incident beam is non-zero. Thus if the surface S is defined as the isointensity contour for which $i(z,x,\lambda) = C \ll i_{\max} = i(0,0,\lambda_0)$ (where C is a constant), the two limiting positions of **H** are given by

$$\mathrm{grad}_S\, i \| \mathbf{H}. \tag{21}$$

Here grad_S is the gradient of the function $i(z,x,\lambda)$ at the

† σ_ν and σ_λ are determined by a least-squares fit of the measured primary beam intensity distribution with expression (13). In the case of σ_ν we have, in fact, used different values for the horizontal and vertical divergences of the beam, $\sigma_{\nu x}$ and $\sigma_{\nu z}$ respectively, in order to obtain a better fit. These two different beam divergences have been introduced in the calculation by replacing σ_ν^2 by

$$\sigma_\nu^2 = \sigma_{\nu x}^2 \sin^2\varphi_m + \sigma_{\nu z}^2 \cos^2\varphi_m$$

in relations (16) to (19), and by

$$\sigma_\nu^2 = \sigma_{\nu x}^2 \cos^2\varphi_m + \sigma_{\nu z}^2 \sin^2\varphi_m$$

in relation (20).

surface S with respect to variables $(k_0)_z$, $(k_0)_x$, $(k_0)_y$, the components of the incident vectors. In the Gaussian approximation defined above the intensity function $i(z,x,\lambda)$ is given by:

$$i = i_0 \exp\{-\alpha_z^2(k_0)_z^2 + \alpha_x^2(k_0)_x^2 + \alpha_\lambda^2[(k_0)_y - k_0]^2\}, \quad (22)$$

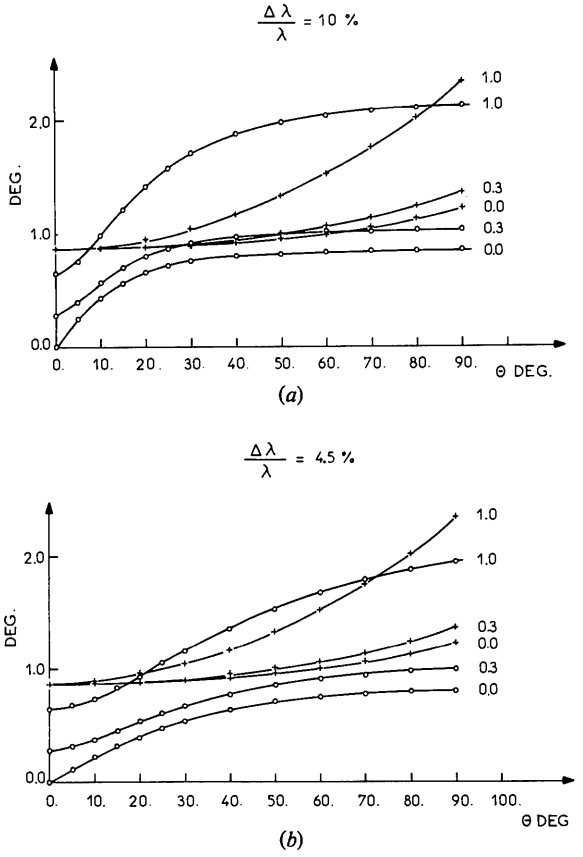

Fig. 4. Variation of the angular width (FWHH) of the diffracted beam as a function of the diffraction angle Θ for three different mosaicities (0, 0·3, 1·0° FWHH): O = radial width, *i.e.* in the direction of the primary beam, + = transversal width, *i.e.* in the direction perpendicular to the first one. (*a*) and (*b*) correspond to wavelength spreads of 10 and 4·5% respectively. Primary-beam divergence 0·87° FWHH.

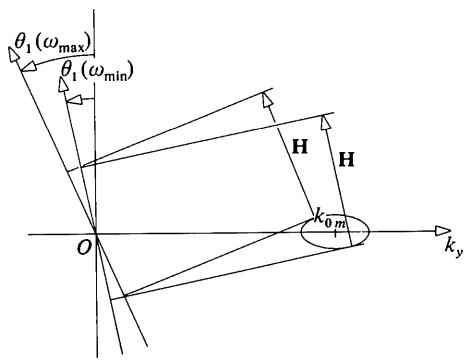

Fig. 5. The two extremes of the diffracting range for a given vector **H** used to determine the ω limits of diffraction for this reflection.

where

$$\alpha_z = 1/k_0\,\sigma_\nu, \quad \alpha_x = 1/k_0\,\sigma_\nu, \quad \alpha_\lambda = \lambda_0/k_0\,\sigma_\lambda. \quad (23)$$

The values of $(k_0)_z$, $(k_0)_x$, $(k_0)_y$ which fulfil (21) are found by solving the following group of equations:

$$\alpha_z^2\frac{(k_0)_z}{H_z} = \alpha_x^2\frac{(k_0)_x}{H_x} = \alpha_\lambda^2\frac{(k_0)_y - k_0}{H_y}$$

$$\alpha_z^2(k_0)_z^2 + \alpha_x^2(k_0)_x^2 + \alpha_\lambda^2[(k_0)_y - k_0]^2 = \ln(1/C)$$

$$H_z^2 + H_x^2 + H_y^2 = H^2, \quad (24)$$

with the result

$$(k_0)_z = \left(\frac{\alpha_\lambda}{\alpha_z}\right)^2\frac{H_z}{H_y}[(k_0)_y - k_0]$$

$$(k_0)_x = \left(\frac{\alpha_\lambda}{\alpha_x}\right)^2\frac{H_x}{H_y}[(k_0)_y - k_0] \quad (25)$$

$$(k_0)_y = k_0 \pm \frac{1}{\alpha_\lambda}[\ln(1/C)]^{1/2} \times\left[1 + \left(\frac{\alpha_\lambda H_z}{\alpha_z H_y}\right)^2 + \left(\frac{\alpha_\lambda H_x}{\alpha_x H_y}\right)^2\right]^{-1/2}.$$

The $\pm$ sign corresponds to the two extreme positions of **H**. To determine the values of ω corresponding to the coordinates given by (25) we use (5) to obtain:

$$[H_x^*(k_0)_y - H_y^*(k_0)_x]\sin\omega + [H_y^*(k_0)_y + H_x^*(k_0)_x]\cos\omega = -H^2/2 - H_z^*(k_0)_z, \quad (26)$$

bearing in mind

$$H_z = H_z^*$$

$$H_x = H_x^*\cos\omega - H_y^*\sin\omega \quad (27)$$

$$H_y = H_x^*\sin\omega + H_y^*\cos\omega.$$

The group of equations (24), (25), (26) is solved together in an iterative manner, starting with $(k_0)_x = (k_0)_z = 0$, $(k_0)_y = k_0$ in (26) to find the first estimate of ω with which to calculate H_x,H_y,H_z in (27).

Effect of mosaic spread. The solutions of the equations given above represent two functions, $\omega_{\min}(H_z^*,H_x^*,H_y^*)$ and $\omega_{\max}(H_z^*,H_x^*,H_y^*)$ which give the two limiting values for a vector **H** of a given crystal. Because of mosaic spread, however, a reflection *hkl* is not described by a single vector **H** but by a whole group of vectors **H** that are related to a mean vector $\mathbf{H}_m$ by small rotations of the angle η (equation 11).

The variation of $\omega_{\min}$ associated with a rotation η about a unit vector **R** is given by:

$$\delta\omega = \eta(\mathbf{R}\times\mathbf{H}_m)\,\text{grad}\,\omega_{\min}. \quad (28)$$

The gradient is calculated by differentiating $\omega_{\min}$ with respect to H_z^*,H_x^*,H_y^* components of $\mathbf{H}_m$. Expression (28) can be rewritten as

$$\delta\omega = \eta\mathbf{R}(\mathbf{H}_m\times\text{grad}\,\omega_{\min}), \quad (29)$$

which shows that, for a given value of η, the variation of $\omega_{\min}$ is largest when the vector **R** is parallel to the vector **H** × grad $\omega_{\min}$. The maximum variation of $\omega_{\min}$ is thus given by

$$\delta\omega = \eta|\mathbf{H}_m + \text{grad } \omega_{\min}|. \tag{30}$$

At a first approximation the values of grad $\omega_{\min}$ and grad $\omega_{\max}$ differ little from the values of grad ω calculated from (26), where the ideal beam with $(k_0)_z = (k_0)_x = 0$; $(k_0)_y = k_0$ is assumed. We thus find, using (27), that

$$\delta\omega = \eta\left[1 + \frac{H_z^2}{H^2(1 - H^2/4k_0^2) - H_z^2}\right]^{1/2}. \tag{31}$$

Within this approximation the value of $\delta\omega$ corresponding to $\omega_{\max}$ is the same as for $\omega_{\min}$, and the ω limits are thus given by:

$$\begin{aligned}\omega_{\min} &= \omega_{\min}(\eta = 0) - \delta\omega \\ \omega_{\max} &= \omega_{\max}(\eta = 0) + \delta\omega,\end{aligned} \tag{32}$$

where the first term on the right is calculated as indicated in the preceding paragraph and $\delta\omega$ is given by (31) taking η as the half-width of the distribution of mosaic spread for a Gaussian distribution (14).

5. Data collection and reduction

5.1. *Determination of mosaic spread*

With the rotation of the crystal, the position of a reflection measured on the detector is displaced according to Θ_m, φ_m. These values depend on the mosaic spread η of the crystal and in order to calculate them *a priori* (equation 17), σ_η has to be determined. This is done, using a small number of strong reflections, by determining experimentally the variation of Θ_m with θ_1 (*i.e.* with ω) and using (18):

$$\sigma_\eta^2 = \frac{1}{\cos\theta_0}\left[(2\sigma_\lambda^{*2} + \sigma_y^2\cos^2\theta_0)\left(\frac{d\Theta_m}{d\theta_1}\right)^{-1} - \sigma_\lambda^{*2} - \sigma_y^2\cos^2\theta_0\right]. \tag{33}$$

When the beam divergence is an order of magnitude larger than the crystal mosaicity, the latter has a negligible effect on the variation of Θ_m with θ_1 as well as on the size of the reflection of the detector. However, for crystals with a mosaic spread commensurate with the beam divergence one can indeed obtain a useful measure of the mosaicity from (33). Equation (18) predicts a nearly linear variation of Θ_m with θ_1, which is indeed found experimentally except towards the limits of the ω range of strong reflections (see Fig. 6). This small discrepancy is not due to the approximations made in deriving (15)–(20), as using the exact expression (12) leads to the same results.

It could be imagined that this effect is caused by the mosaicity distribution tending to zero more slowly at its extremes than a Gaussian function (14) would. To test this hypothesis we tried a mosaicity distribution represented by the sum of two Gaussians, a principal narrow one and a second broader one with smaller weight. The results obtained are not always satisfactory. A careful analysis of the data indicates that

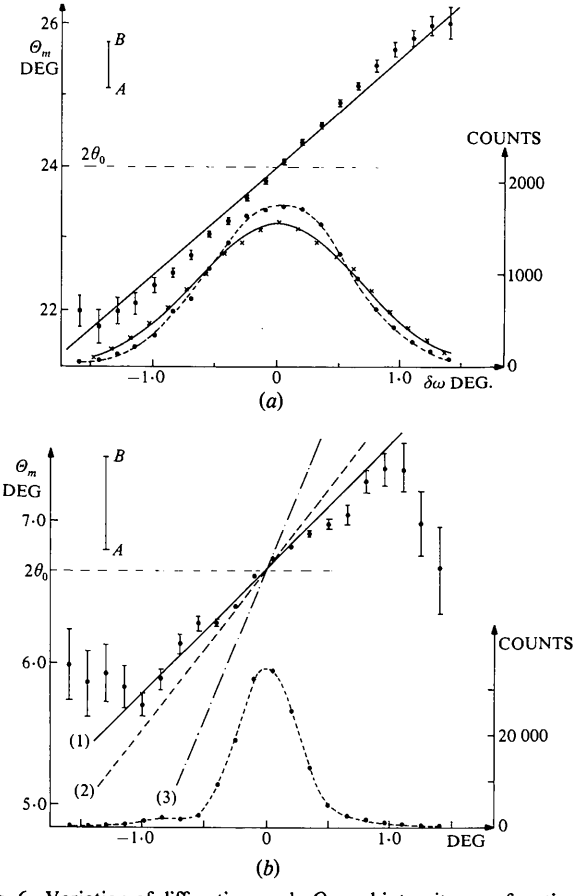

Fig. 6. Variation of diffraction angle Θ_m and intensity as a function of rotation angle ω (in fact $\delta\omega$, which is the offset ω with respect to its mean value for the reflection used here). Experimental points •. Upper part of figures and left-hand ordinate scale: $\Theta_m(\omega)$. Straight lines were calculated with relation (18); θ_0 is the mean Bragg angle; the length AB represents 1 cm on the detector. Lower part and right hand scale: variation of total intensity. Dashed line experimental curve; full line theoretical curve calculated with relation (15); points × are calculated with relation (9) by numerical integration over Θ,φ. (*a*) An example of a case where mosaicity is negligible ($\sigma_\eta \simeq 0$): the deviation of experimental points from theoretical curves comes from the hypothesis that the wavelength distribution in the primary beam is independent of **x** and **z**. (*b*) The influence of mosaicity on $\Theta_m(\omega)$: straight lines (1) and (2) correspond to mosaicities of 0·5 and 0·0° (FWHH) respectively. Line (3) represents the ideal $(\theta,2\theta)$ variation. The deviation of Θ_m from a straight line as well as the long 'wings' on the intensity curves are very likely due to phonon scattering, measured on this extremely intense reflection.

this anomaly is due to part of the measured intensity being in fact phonon scattering.

5.2. *Calculation of integration masks and background determination*

To calculate the mask of a given reflection in a given spectrum, a square integration box of a fixed size (typically 5 to 11 cm a side) is positioned around the reflection using the predicted coordinates Θ_m, θ_m. The theoretical relative intensity $\delta n(\Theta,\varphi)$ (equation 15) is then calculated for each cell within this box. The cells for which the value of δn is found to be larger than the threshold value C are retained for intensity integration; the remaining cells serve to determine the background. For each reflection of the crystal, C is given a different value in order to adapt the size of the masks of the reflection to its real intensity:

$$C \sim C_0 \sigma_{BG}/I_{\max}, \tag{34}$$

where $I_{\max}$ is the maximum intensity of the reflection, σ_{BG} the standard deviation of the background and C_0 is a numerical constant smaller than 1. The value of C_0 was derived from the following considerations: in the Gaussian approximation, the theoretical systematic error that is introduced by integrating the intensity up to the threshold C is equal to CI_c. Here I_c would be the exact integrated intensity of the reflection. We can assume that the reflection will be integrated without bias if the value of CI_c is smaller than σ_I, the standard deviation of I_c. We have therefore

$$CI_c < \sigma_I. \tag{35}$$

The systematic error given by CI_c is independent of the actual intensity of the reflection. It is a function of C_0 and of the ratio

$$r = I_c/I_{\max}. \tag{36}$$

The value of σ_I, on the other hand, increases with intensity. The condition (35) is therefore fulfilled for all reflections if it holds for the weakest ones. In this latter case we can consider

$$I_{\max} \sim \sigma_{BG} \tag{37}$$

and approximate σ_I by

$$\sigma_I \sim \sqrt{m}\,\sigma_{BG}, \tag{38}$$

where m is the number of detector elements used for the intensity integration. For weak reflections this number is significantly smaller than the number of cells used for background determination. It can be shown that in the Gaussian approximation used the value of m is given by

$$m \sim \frac{2r}{3\sqrt{\pi}} (\log 1/C)^{3/2}. \tag{39}$$

The value of r can be predicted by integrating δn (equation 15). A value of C_0, for which inequality (35) is fulfilled, is finally obtained from

$$C_0 = \left(\frac{3\sqrt{\pi}\, r}{2}\right)^{-1/2}. \tag{40}$$

For a typical value of $r = 10$, we have $C_0 = 0{\cdot}2$. The values of $I_{\max}$ are determined experimentally from the spectrum closest to the ω value where the reflection has its maximum intensity (*i.e.* $\theta_1 \sim \theta_0$), using a fit of the measured intensity against the theoretical value of $\delta n(\Theta,\varphi)$. The average background per cell is determined from the local background in the vicinity of a reflection. It is estimated from cells within the integration box of a given reflection. Since several reflections can, in fact, be found at least partially in the same integration box, it is necessary to proceed in two steps. First the masks for all reflections occurring on a spectrum are calculated. The background for a reflection is then determined within the integration box of that reflection using the cells that are not used for any mask. The integration boxes are chosen large enough to allow a sufficient number of cells to be used for background. The precalculation of reflection masks for each spectrum allows, at the same time, an easy detection of overlap where that occurs.

6. Test of the integration method

The data reduction system was tested on data from a crystal of the nucleosome core particle soaked in a standard (H_2O) buffer (Bentley, Finch & Lewit-Bentley, 1981). The crystal was orthorhombic, space group $P2_12_12_1$, with cell dimensions $a = 111$, $b = 198$, $c = 111$ Å, and crystal dimensions $1 \times 0{\cdot}45 \times 0{\cdot}35$ mm. The wavelength used was $\lambda = 9{\cdot}25$ Å with $\Delta\lambda/\lambda = 10\%$; crystal-to-detector distance $D = 154{\cdot}5$ cm, detector angle $\kappa = 13°$. The data extend to ~25 Å d spacing for fully recorded reflections. In order to collect a full data set to this resolution, with on the average two equivalents for each reflection, we measured a total crystal rotation of 136° using 0·15° steps. The time per step averaged 6 min. The detector cell size used was 1×1 cm, thus producing spectra of 4096 data per step. The beam dimensions were $\sigma_x = 0{\cdot}61$, $\sigma_y = 1{\cdot}59$ cm; the crystal mosaic spread parameter was $\eta = 0{\cdot}0°$.

The data were processed on the PDP-10, 1070 computer at the ILL where the program takes about 80K core. For example, a set of 85 spectra of 4K with a total of 32 fully recorded reflections (over 12·3° in ω) took 232 s of CPU time.

For comparison, two other data-reduction programs were used:

(1) a program based on the full formulation of the resolution function (*i.e.* equation 12). The only disadvantage of this program is that it is at least ten times slower.

(2) a program (written by G. A. Bentley) based on a simple model for the shape of a reflection in reciprocal space (the 'square-box' method). The mosaic spread of the crystal and the beam divergence are accounted for together by giving the reciprocal-lattice point a spherical volume of radius η. The wavelength spread is accounted for by assuming a range of wavelengths of $\lambda_{mean} +/- 2\Delta\lambda$. The X,Y detector coordinates and the ω range are calculated as suggested by Wonacott (1977). The shift of a reflection centre during an ω scan is assumed linear and individual X,Y coordinates interpolated between the limiting positions. The actual value of η is determined by trial-and-error using a large enough sample of reflections. On each spectrum the integration of intensity is performed over a square box of size chosen so as to contain the reflection at its maximum but to avoid overlap. Background is determined from a row of detector cells along each edge of the square. These rows of cells are checked for anomalies (*e.g.* overlap) and flagged.

As can be seen from Table 1, the results using the resolution function, whether in its full form or the Gaussian approximation, are very similar. The 'square box' method gives a worse agreement between symmetry equivalents. The inflexibility of a square integration box means that reflections close to detector edges will be rejected as partially recorded when in fact they could be integrated (and are with the resolution function). The same inflexibility causes problems for crystals with larger unit-cell dimensions as the integration squares start overlapping. The lower part of Table 1 demonstrates that the resolution function is most useful for determining weak intensities, where the discrimination between peak and background can be otherwise very difficult.

The last column in Table 1 shows the results for data measured more recently on the same H_2O nucleosome core particle crystal, using $D = 81{\cdot}3$ cm, $\lambda = 11{\cdot}87$ Å, $\Delta\lambda/\lambda = 10\%$, $\sigma_x = 0{\cdot}75$ cm, $\sigma_y = 0{\cdot}87$ cm, $\eta = 0{\cdot}0°$. The detector angle κ was 22°, with the main beam on the edge of the detector. In total, 1712 spectra of 4K each were collected, over a scan of 256·5° with 0·15° steps in ω. The measuring time averaged 3 min step^{-1}. In this way, each unique reflection to a d spacing of ~16·5 Å was measured two to six times.

Fig. 7 is an example of these data. It illustrates well the behaviour of reflections due to the wavelength spread: the centre of gravity of reflection 115 shifts by some 6 cm across the detector between its peak position at $\omega = 202{\cdot}25°$ and its end at $\omega = 204{\cdot}35°$. Some reflections are separated by as little as one row of background cells. Depending on the unit-cell dimensions, as many as 25 to 120 reflections (for a 111 × 198 × 111 Å primitive cell and a 354 × 354 × 354 Å body-centred cell respectively) can be active on a single spectrum.

All data were corrected with a Lorenz factor for normal beam geometry, applicable to ideal diffraction conditions. We have verified that, in spite of the non-ideal conditions, the same results are obtained using a Lorenz factor derived from (12).

Conclusion

The data reduction method described is well adapted to a data-collecting system using cold neutrons when, because of the large wavelength spread used, the position and size of a given reflection vary over a wide

Table 1. *Comparison of intensity data obtained by different integration methods*

	Data to 25 Å d spacing			Data to 16·5 Å d spacing
	Complete resolution function	Gaussian resolution function	Square-box approximation	Gaussian resolution function
Total number of reflections fully recorded	220	218	207	832
Total number of unique reflections	119	118	113	282
R_{sym} on common reflections (201 reflections)	0·023	0·023	0·029	0·032

R_{sym} for reflections	Gaussian		Square box		16·5 Å data	
	R_{sym}*	Number of reflections	R_{sym}	Number of reflections	R_{sym}	Number of reflections
0σ–3σ	0·44	24	0·47	22	0·49	182
3σ–6σ	0·18	36	0·19	42	0·16	118
6σ–9σ	0·09	18	0·12	18	0·12	122
9σ–12σ	0·08	12	0·04	4	0·10	48
above 12σ	0·015	74	0·018	78	0·02	295

* $R_{sym} = \sum_{hkl} \sum_{i=1}^{N} |I(hkl)_i - \langle I(hkl)\rangle| / \sum_{hkl} \sum_{i=1}^{N} |I(hkl)_i|$ (Spencer & Kossiakoff, 1980).

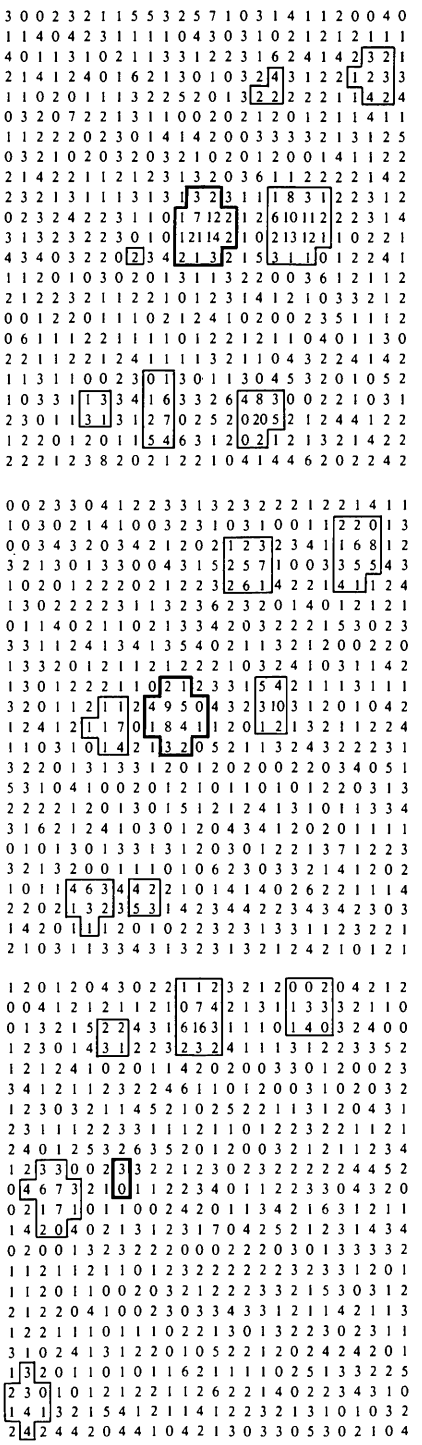

Fig. 7. Example of masks calculated for the more recent data from the nucleosome core-particle crystals. The top left-hand part of the detector is shown. The coordinates of the detector elements run from 6 to 31 along the top and from 52 to 30 down the left-hand side. Three angular settings of the crystal are illustrated: $\omega = 202{\cdot}25°$ (top), $\omega = 203{\cdot}0°$ (middle), and $\omega = 204{\cdot}35°$ (bottom). The reflections shown are, from left to right and top to bottom: 215, 214 and 216 appearing at $\omega = 204{\cdot}35°$; 116, 115 and 114; 016, 015 and 014 disappearing at $\omega = 204{\cdot}35°$. Reflection 115 is outlined in heavy lines.

range when the reflection is scanned. The use of this method has shown that it gives, with very simple mathematics, a good prediction of the value of these parameters and an easy adaptation of the size to the real intensity of the reflection. Reflections very close to each other can be easily discriminated and weak reflections collected in a safe way. The algorithms involved in computing are rather simple and fast.

The successful application of the resolution function depends on the knowledge of the primary-beam intensity distribution, which can be determined from a simple direct measurement. The crystal orientation matrix and mosaicity must also be known. If, however, the beam divergence is significantly larger than the mosaic spread of the crystal, the resolution function becomes essentially independent of the mosaicity parameters. This is in fact the case for most crystals, using the standard conditions on D17, with $D = 80$ cm and beam divergence of 1°.

The scientific interest of this kind of method is that it is based on a theoretical calculation of diffracted intensity. Any marked departure of experimental data from the calculated intensity has to be given a physical explanation which demands careful analysis of what is actually measured. Thus we have detected, in the proximity of very intense reflections (Fig. 6*b*), peaks due very likely to phonon scattering.

The quality of the data measured so far suggests that a gas-filled multiwire multidetector, when properly calibrated, is an adequate detector for diffraction data.

We would like to thank G. A. Bentley for many helpful discussions and constant help and advice during the development and testing of the method.

References

BENTLEY, G. A., FINCH, J. T. & LEWIT-BENTLEY, A. (1981). *J. Mol. Biol.* **145**, 771–784.

BUSING, W. R. & LEVY, H. A. (1967). *Acta Cryst.* **22**, 457–464.

COOPER, M. J. & NATHANS, R. (1967). *Acta Cryst.* **23**, 357–367.

COOPER, M. J. & NATHANS, R. (1968). *Acta Cryst.* A**24**, 481–484.

IBEL, K. (1976). *J. Appl. Cryst.* **9**, 296–309.

LEBECH, B. & NIELSEN, M. (1975). Neutron Diffraction Conference, Petten, The Netherlands.

LOMER, W. M. & LOW, G. G. (1965). *Thermal Neutron Scattering*, edited by P. A. EGELSTAFF, p. 18. London, New York: Academic Press.

SJÖLIN, L. & WLODAWER, A. (1981). *Acta Cryst.* A**37**, 594–604.

SPENCER, S. A. & KOSSIAKOFF, A. A. (1980). *J. Appl. Cryst.* **13**, 563–571.

WONACOTT, A. J. (1977). *The Rotation Method in Crystallography*, edited by U. W. ARNDT & A. J. WONACOTT, pp. 75–103. Amsterdam: North Holland.

XUONG, N. H., FREER, S. T., HAMLIN, R., NIELSEN, C. & VERNON, W. (1978). *Acta Cryst.* A**34**, 289–296.